Chemical Geology 587 (2022) 120608

Contents lists available at ScienceDirect

Chemical Geology

journal homepage: www.elsevier.com/locate/chemgeo

Disentangling diagenetic and biogenic trace elements and Sr radiogenic isotopes in fossil dental enamel using laser ablation analysis

Léonie Rey [a], Théo Tacail [b], Frédéric Santos [a], Stéphane Rottier [a], Gwenaëlle Goude [c], Vincent Balter [d,*]

[a] CNRS UMR 5199, PACEA, Univ. Bordeaux, Allée Geoffroy Saint Hilaire, CS 50023, 33615 Pessac Cedex, France
[b] Bristol Isotope Group, School of Earth Sciences, University of Bristol, Bristol BS8 1RJ, UK
[c] Aix Marseille Univ, CNRS, Minist Culture, LAMPEA, Aix-en-Provence, France
[d] CNRS UMR 5276, LGLTPE, Univ. Lyon, ENS de Lyon, Univ. Lyon1. 46, Allée d'Italie, 69342 Lyon Cedex 07, France

ARTICLE INFO

Editor: Christian France-Lanord

Keywords:
Laser ablation
Trace elements
Strontium isotopes
Neolithic
Diet
Mobility
Enamel
Bone

ABSTRACT

The reconstruction of life histories traits such as the ontogenic evolution of diet or sequences of mobility can be achieved for fossil mammals thanks to laser ablation analysis of trace elements concentration and radiogenic Sr isotope composition in dental enamel. However, a major limitation for the use of laser ablation to study fossil tooth enamel is that the analysis must be carried out on bulk sample hence prohibiting any ad hoc leaching step to remove diagenetic compounds. Biogenic and diagenetic trace elements along with the $^{87}Sr/^{86}Sr$ ratio must be monitored and post hoc correlation tests processed to isolate areas free of diagenesis. The present study combines a unique combination of biogenic (Sr and Ba), diagenetic (Mn and U) trace elements, major elements (Mg and Ca) and $^{87}Sr/^{86}Sr$ ratio time series obtained by means of laser ablation ICPMS and MC-ICPMS on a large number ($n = 94$) of fossil tooth enamel samples of humans and animals from a set of neighboring Neolithic sites in France. Bone fragments sampled from the same specimens are also analyzed for comparison. Trends between diagenetic and biogenic trace and major elements are first identified using inclusive data analysis. The trends are then validated at the scale of the laser ablation raster, and a protocol of data cleaning is developed to identify areas free of diagenesis. Non-significantly altered Sr/Ca, Ba/Ca and $^{87}Sr/^{86}Sr$ average values are thus gathered for each cleaned tooth enamel samples and are discussed, along with previously measured bone collagen $\delta^{13}C$ and $\delta^{15}N$ values, in terms of diet and mobility in the context of the Neolithic revolution.

1. Introduction

The analysis of trace elements and radiogenic strontium isotopes in fossil bone and teeth to reconstruct ancient diet and mobility is nowadays of routine use in bioarchaeology and paleoanthropology. Of particular interest for ancient mammal dietary habits is the analysis of fossil enamel strontium/calcium ratio (Sr/Ca) and barium/calcium ratio (Ba/Ca). Sr and Ba are discriminated against Ca in biochemical pathways, which include Ca as an essential element, resulting in the overall decrease of the Sr/Ca and Ba/Ca ratios up trophic chains and allowing the reconstruction of ancient dietary behaviors (e.g., Austin et al., 2013; Balter et al., 2001; Gilbert et al., 1994; Joannes-Boyau et al., 2019; Sponheimer and Lee-Thorp, 2006). The radiogenic ^{87}Sr isotope abundance is determined after normalization of the stable isotope variations to a reference $^{88}Sr/^{86}Sr$ value, therefore the $^{87}Sr/^{86}Sr$ ratio is immune to biological and any other process up the trophic chain. Consequently, the $^{87}Sr/^{86}Sr$ ratio of an animal ultimately reflects that of the bedrock on which it feeds and is used for the reconstruction of ancient mobility (e.g., Sillen et al., 1998; Müller et al., 2003; Balter et al., 2012; Sillen and Balter, 2018; Lugli et al., 2019).

Since the very beginnings of this archeometric discipline, diagenesis has been recognized to be a major limitation and two methods have been developed to overcome this problem. The first method is to leach ad hoc the bone or enamel sample with dilute acetic acid to remove secondary Ca-carbonates (e.g., Balter et al., 2002; Hopkins et al., 2016; Nelson et al., 1986). However, Ca-carbonates are not the only potential secondary phase, oxy-hydroxides being also frequent diagenetic phases, which are not removed by acetic acid. In addition, bone or enamel can be recrystallized, an extreme case where any leaching technique is helpful. The second method consists to monitor the concentration of an

* Corresponding author.
E-mail address: vincent.balter@ens-lyon.fr (V. Balter).

https://doi.org/10.1016/j.chemgeo.2021.120608
Received 27 July 2020; Received in revised form 9 September 2021; Accepted 27 October 2021
Available online 1 November 2021

element which is known to be of diagenetic origin and perform post hoc correlation tests with the elements (mainly Sr and Ba) supposed to be of biogenic origin. Uranium (U), thorium (Th) and Rare Earth Elements (REE) accumulate in fossil bones and teeth (Kohn et al., 1999; Reynard and Balter, 2014), and are good indicators of the intensity of the diagenesis. The influence of oxy-hydroxides on the biogenic elements concentration can easily be assessed by measuring manganese (Mn) concentration (e.g., Reynard and Balter, 2014). Regarding the $^{87}Sr/^{86}Sr$ ratio, the existence of a correlation between the concentrations and isotope compositions along a mixing hyperbola will attest of a diagenetic overprinting (Budd et al., 2000; Martin et al., 2016).

Thanks to the development of laser ablation, it is now possible to analyze in situ the trace elements concentration (Dolphin et al., 2005; Humphrey et al., 2008; Kohn et al., 2013; Müller et al., 2019) and the $^{87}Sr/^{86}Sr$ ratio (e.g., Balter et al., 2008; Lugli et al., 2017; Montgomery et al., 2010). This is of noteworthy interest for enamel because it is less sensitive to diagenesis than bone thanks to its less porous structure, and because it grows incrementally, allowing the reconstruction of individual dietary and mobility histories (Austin et al., 2013; Balter et al., 2012; Joannes-Boyau et al., 2019). However, there is a major limitation for the use of laser ablation of fossil tooth enamel, which is that the leaching step is not possible because it needs to be carried out on powdered samples. Biogenic and diagenetic trace elements must be monitored along with the $^{87}Sr/^{86}Sr$ ratio and post hoc correlation tests processed to determine the areas free of diagenesis. To the best of our knowledge, this has been done in three studies only (Balter et al., 2012; Simonetti et al., 2008; Willmes et al., 2016), but no trace elements and radiogenic Sr systematics in fossil tooth enamel has been done yet using laser ablation.

The present study combines a unique set of biogenic (Sr and Ba), diagenetic (Mn and U) trace elements, major elements (Mg and Ca) and $^{87}Sr/^{86}Sr$ ratio time series obtained by means of laser ablation ICPMS and MC-ICPMS on a large number of fossil tooth enamel samples ($n = 62$ and 32 for humans and animals, respectively) from a set of neighboring Neolithic sites in France. Bone samples of same specimen are also analyzed for comparison. In the archaeological context of Neolithic Revolution, which is one of the biggest socio-cultural transitions in human history, dietary behavior and mobility of human groups are central issues because people settled down building villages and hunter-gatherers became farmer-pastoralists. The use of laser ablation in such an archaeological and chrono-cultural context is a crucial methodological step that will pave the way for studies on longitudinal life histories.

Laser ablation measurements of trace elements concentrations and $^{87}Sr/^{86}Sr$ ratios produced in the present study a large number of data (> 500,000). Global trends between diagenetic and biogenic trace and major elements are first identified using inclusive data analysis. These trends are then validated at the scale of the laser ablation raster, and a protocol of data cleaning is developed to identify areas free of diagenesis and with reliable $^{87}Sr/^{86}Sr$ ratio. Most of the rasters unfortunately exhibit diagenetic portions so that the full time series are not exploitable. Non-significantly altered Sr/Ca, Ba/Ca and $^{87}Sr/^{86}Sr$ average values are thus gathered for each tooth enamel and bone samples and are discussed, along with previously measured bone collagen $\delta^{13}C$ and $\delta^{15}N$ values.

1.1. Material

The bone and tooth enamel samples come from seven Neolithic sites within a radius of 10 km along the Yonne valley, in the South-East of the Paris basin, at the Northern edge of the Morvan massif, France (Fig. 1). The sites with the corresponding material are presented in Table 1. They are dated to different and overlapping periods covering the 5th millennium BCE and they refer to different and mixed cultural spheres (Table 1). Further archaeological details are available in Rey et al. (2019). The bioavailable Sr local range is determined on the grounds of the geological variability from plants and soil samples given by the iRhum database regionally (within a 15 km radius around the sites, including layers q3, q2, c1, c2 and j3; Fig. 1), and is found to vary from 0.7075 to 0.7145 (Willmes et al., 2013). For humans, all the teeth are second molar (M2) except for 2 individuals for whom the teeth are first molar (M1). This corresponds to a life history between approximately 2.5 and 8.5 years ± 0.5 for M2 and between approximately 0.5 and 3.5 years ± 0.5 for M1 (AlQahtani et al., 2010). When it was possible, bone from the same individual was also analyzed to assess dietary and mobility changes between childhood and adulthood because bone records a signal corresponding to the individuals' last years of life (Hedges et al., 2007; Szulc et al., 2000) and to assess potential differential diagenetic sensitivity relative to enamel.

All observations (anatomical variations, pathologies, stress indicators, wear, maturation stage) and external metrics were recorded and teeth pictured. In addition, calculus samples, impressions of the crown and µCT-scans were computed whenever possible for further complementary studies (Le Luyer et al., 2016; Rey et al., 2016). The teeth were cut in two pieces with a diamond saw, along the longitudinal bucco-lingual axis, passing through the top of the mesial cusps and

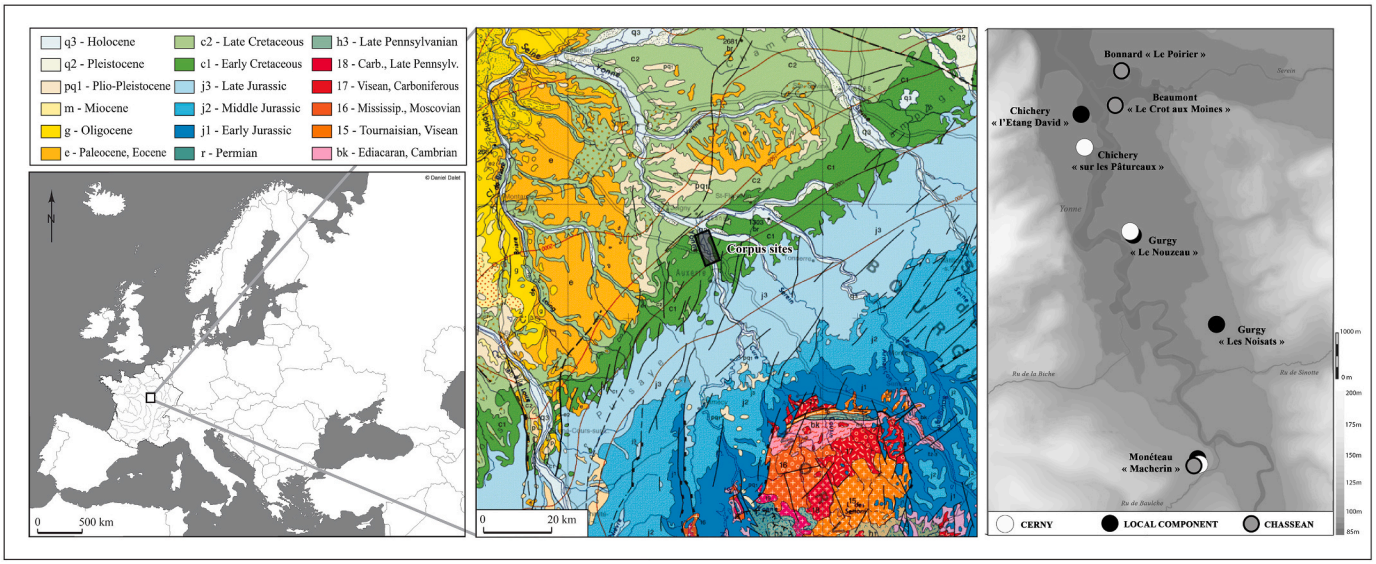

Fig. 1. Localization of the sites and regional geological map. Information is from geoportail.gouv. Scale 1/1,000,000.

Table 1
Summary of archaeological sites information and samples provenance.

Code site	Name site	Cultural attribution	^{14}C date	Spatial organization	Number of humans buried	Animal remains	Enamel samples	Bone samples	Stable isotopes[b]
NZ	Gurgy "Le Nouzeau"	Cerny (+ local)	5300–4700 cal BC	enclosure with scattered remains +2 associated burials	2 + scattered remains	yes	2 humans 1 animal	2 humans 2 animals	CNS
GLN	Gurgy "Les Noisats"	local component?	5200–3800 cal BC	big and dense cemetery	128	yes	34 humans 8 animals	12 humans 6 animals	CNS
Mon	Monéteau "Macherin"	Chassean (+Cerny +local)	5200–3500 cal BC?	cemetery divided in separated groups	62	no	13 humans	2 humans	CNS
CHI-ED	Chichery "l'Etang David" [a]	local component?	5100–4100 cal BC	cemetery partially destroyed	20	no	1 human	1 human	CN
CHI-Pat	Chichery "Sur les Pâtureaux"	Cerny	4700–4350 cal BC	funerary site with aligments of burials +1 isolated burial	15	no	6 humans	3 humans	CNS
BMT	Beaumont "Le Crôt aux Moines" [a]	Chassean	4800–4000 cal BC	enclosure with scattered remains + other structures	scattered remains	yes	2 humans 18 animals	12 animals	CNS
Bon	Bonnard "Le Poirier" [a]	Chassean	4500–4000 cal BC	2 burials of several inhumations	6	no	1 human	none	CN

[a] Ancient excavation.
[b] Rey et al., 2017; Rey et al., 2019.

perpendicular to the collar (crown root junction, or crj). The mesial part was embedded, with a bone fragment from the same individual whenever possible. Bone fragments were taken from long bone cortical fragments (the bone type is indicated in table S1). The fragments were surface cleaned with a sandblaster with aluminium oxides, washed by compressed air, embedded with tooth enamel in epoxy resin and finally polished manually (granulometry P4000) to obtain a smooth surface.

2. Method

2.1. Laser ablation

In tooth enamel, rasters were processed along the enamel dentine junction (edj) to cross the Retzius' striae and the transverse striations. For humans and pigs, the profiles were drawn from the apex (« ocl ») to the crj (« col. »). The rasters for concentration and isotopic composition were as close as possible. In bone, one or two small rasters were processed to obtain sufficient data to average. Samples were run according to a fixed sequence procedure according to Tacail et al. (2017). Each sequence was composed of 3 to 6 samples and was bracketed by a sintered international standard SRM1400 "bone ash" (Tacail et al., 2016) at the beginning and the end of the sequence to correct for instrumental biases. Blank was measured during 5 s (laser off) before each measurement. The laser ablation device was connected to a quadrupole-ICPMS (Q-ICPMS, X series, ThermoFisher) for the measurement of element concentrations and to a multicollector-ICPMS (MC-ICPMS, Nu500 HR, Nu Instruments) for the measurements of Sr isotopes. The spot size for the acquisition of trace elements and Sr isotopes was respectively 50 and 150 μm, with a frequency of 10 and 20 Hz and a speed of 10 μm/s for both. Operating conditions are summarized in Table 2.

Table 2
Instruments settings.

Laser (Excite 193 nm, photon machine)	
LA pulse [ns]	<4
He MFC1 [L.min^{-1}]	0.8
He MFC2 [L.min^{-1}]	0.4
Laser Output [%]	100
Rep Rate [Hz]	10
Spot Size [μm]	50/150
Scan speed [μm]	10
ICPMS (X Series, ThermoFisher)	
RF-power [W]	1350
Ar gas flow	
Sample [L.min^{-1}]	1
Coolant [L.min^{-1}]	13
Auxiliary [L.min^{-1}]	0.8
Analyzed isotopes	^{24}Mg, ^{43}Ca, ^{55}Mn, ^{88}Sr, ^{138}Ba, ^{238}U
MC-ICPMS (Nu Plasma HR, Nu Instruments)	
RF-power [W]	1400
Cones	Ni
Gas flow	
He Sample [L.min^{-1}]	1
Ar Coolant [L.min^{-1}]	13
Ar Auxiliary [L.min^{-1}]	0.7
Cup configuration	H4(^{88}Sr), H2(^{87}Sr + ^{87}Rb) Ax(^{86}Sr + ^{86}Kr), L2(^{85}Rb) L3(^{84}Sr + ^{84}Kr), L4(^{83}Kr)

2.2. Data processing

The laser ablation technique generates a considerable amount of data that must be treated and reduced before being interpreted accurately. Each sequence (two standards bracketing 2–3 samples) corresponds to a single block of measurements, either on the Q-ICPMS and MC-ICPMS. These raw data sequences were semi-automatically processed with Spyder Python 2.7 software to obtain corrected profiles for each sample. The procedure notably detects and isolates samples and standards measurements using blanks (5 s) that are added between each sample or standard. The procedure for element concentration is fully described in Tacail et al. (2017). For Sr isotopes, the measurements were corrected using the classical ^{85}Rb and ^{83}Kr corrections and the ^{87}Sr/^{86}Sr ratio of the samples was subsequently normalized by the bracketing SRM1400 standards with a factor depending on their position relative to the standards. Because ICPMS and MC-ICPMS have dramatically different data integration time, we use relative position expressed as percent of the raster length to match trace elements concentration and Sr isotope composition at a given location. Elemental ratios are expressed relative to Ca*1000 otherwise specified. Statistical analyses were performed using the FactoMineR and PerformanceAnalytics packages of the R software.

3. Results and discussion

3.1. Quality control of the measurements

As previously mentioned, we used a sintered international standard SRM1400 "bone ash" (Tacail et al., 2016) at the beginning and the end of the sequence to correct samples for instrumental biases. A total of 98 and

140 measurements of the SRM1400 standard has been processed for Sr isotopes and trace elements, respectively. Ablation of the SRM1400 standard, certified to contain 250 ppm of Sr, produces here a signal for ^{88}Sr of ≈0.9 V on the MC-ICPMS and of ≈140,000 cps on the Q-ICPMS. The average value of the ^{87}Sr $^{/86}$Sr ratio is 0.71310 ± 0.00218 (2SD, n = 98) very close to the TIMS value of 0.71308 ± 0.00005 (2SD, n = 25; Brazier et al., 2020). The average value of the Sr/Ca, Ba/Ca and Mg/Ca ratios are 0.653 ± 0.038, 0.630 ± 0.049 and 17.93 ± 0.73, respectively, which are always very close to certified values (0.652 ± 0.018, 0.629 ± 0.026 17.91 ± 0.35, for Sr/Ca, Ba/Ca and Mg/Ca, respectively; Balter and Lécuyer, 2004).

3.2. Bulk radiogenic Sr isotope compositions

The standard deviation of standard and sample corrected ^{87}Sr/^{86}Sr ratios are plotted as a function of the ^{88}Sr voltage in Fig. 2A and show an increase of the variability as the ^{88}Sr voltage decreases, a pattern that has been recognized by Horstwood et al. (2008). Comparing the discrepancy between laser ablation and solution ^{87}Sr/^{86}Sr measurements, Simonetti et al. (2008) and Copeland et al. (2008) have also observed that the accuracy of the laser ablation measurements decreases with Sr total voltage. The decreasing ^{88}Sr voltage is also accompanied by an increase of the corrected ^{87}Sr/^{86}Sr ratios mean values (Fig. 2B). Horstwood et al. (2008) and Simonetti et al. (2008) argued that the increase of the ^{87}Sr/^{86}Sr ratio is due to a ^{40}Ca-^{31}P-^{16}O polyatomic interference at mass 87. However, using Sr/Rb-free concentrated Ca/P solutions, Müller and Anczkiewicz (2016) recently demonstrated that the ^{40}Ca-^{31}P-^{16}O polyatomic interference does not occur at the required intensities to explain the observed increase of the ^{87}Sr/^{86}Sr ratio. Horstwood et al. (2008) proposed that the complete elimination of this interference should be achieved using rigorous calibration to known reference materials, which is actually not the case given the present results. The increase of the variability of the ^{87}Sr/^{86}Sr ratio is likely due to degraded counting statistics for too low voltage. The concomitant increase of the average value of the ^{87}Sr/^{86}Sr ratio with decreasing Sr voltage remains unexplained, but must be ultimately linked, at least indirectly, to degraded counting statistics and thus, could not be corrected anyway. We have selected a threshold value at 0.4 V for ^{88}Sr below which the value of the ^{87}Sr/^{86}Sr ratio is considered inaccurate and thus eliminated for further discussion. This value holds for a Nu Plasma HR MC-ICPMS and should be different for a Neptune instrument. We also note that there is an apparent increase of the variability of the ^{87}Sr/^{86}Sr ratio for ^{88}Sr voltage ≥1 V (Fig. 2A), but which does not seem to be followed by an increase, or a decrease, of the average value (Fig. 2B). The analysis of the ^{87}Sr/^{86}Sr ratio in bone and tooth enamel by laser ablation should be adapted for each sample, by varying the diameter of the spot size and/or the sampling rate of the laser to obtain enough signal that should ideally lie between 0.6 V to 0.9 V for ^{88}Sr.

3.3. Bulk trace elements compositions

The dataset has been explored using principal component analysis (PCA). PCA consists in reducing the dimensionality of dataset while preserving most of the information. The basic representation provides eigenvectors of the covariance matrix in two dimensions, the principal components (PCs) which are the new variables. Co-variation of the eigenvectors yields information about correlation of the variables. PCA are particularly useful for large dataset, such as in the present study which considers six independent variables (Mg, Ca, Mn, Sr, Ba and U) representing ~450,000 and 50,000 measurements for enamel and bone, respectively. We have first performed PCA on the whole dataset (Fig. 3A and B). For enamel, the first two PCs account for 31.7% and 21.6%, respectively, of the total variation in the dataset, so the two-dimensional scatterplot given by Fig. 3A represents 53.3% of the variance of the original eleven-dimensional space. All eigenvectors except Mg/Ca are positive along PC1, indicating that they are all positively correlated and negatively correlated to Mg/Ca. Along PC2, eigenvectors of biogenic (Mg, Ca, Sr, Ba and related Ca-ratios) and diagenetic (Mn, U and Ca-ratios) variables are clustered indicating that the set of data contains clear biogenic and diagenetic components that intrinsically positively correlated. The direction of the Mg/Ca eigenvector is opposed to that of U/Ca demonstrating that these ratios are strongly anti-correlated. The direction of the Sr/Ca and Ba/Ca eigenvectors is approximately perpendicular to those of Mn/Ca and U/Ca ones, indicating that the biogenic and diagenetic variables are not correlated. To resume, the information carried by the PCA on enamel suggests that the Sr/Ca and Ba/Ca ratios are not correlated with those of Mn/Ca and U/Ca and that the Mg/Ca ratio negatively correlated to the U/Ca and of Mn/Ca ratios. These conclusions apparently hold for bone, except that the Mg/Ca ratio is positively correlated to those of Sr/Ca and Ba/Ca (Fig. 3B). However,

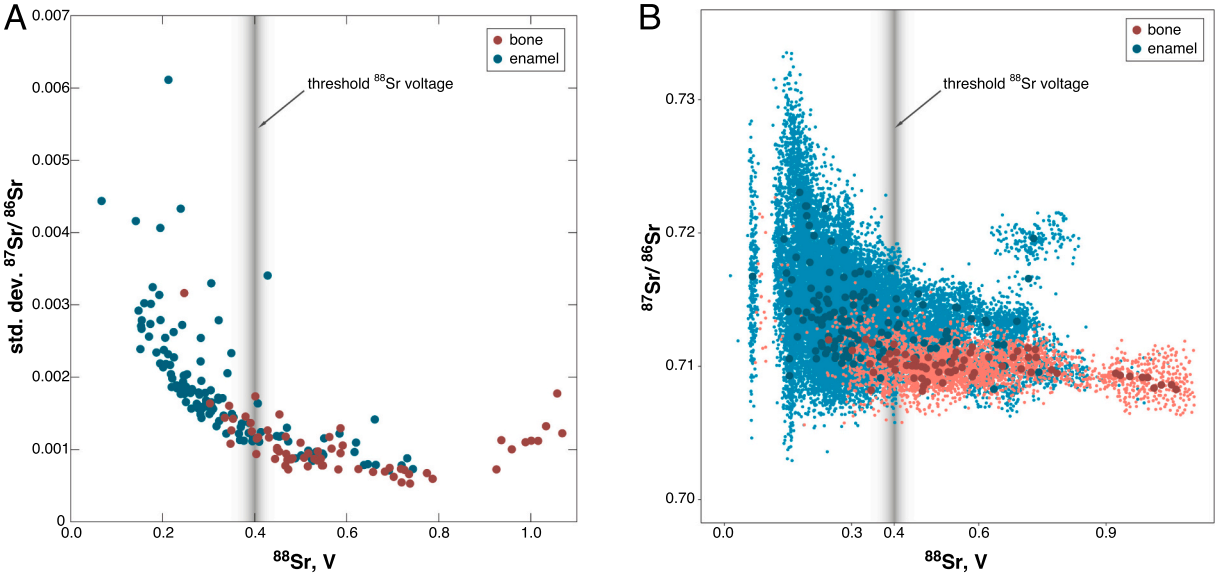

Fig. 2. Quality control of Sr radiogenic isotopes. A) Scatterplot of the standard deviation of the ^{87}Sr/^{86}Sr ratio a function of the ^{88}Sr voltage showing an increase of the variance with decreasing voltage. B) Scatterplot of the standard deviation of the ^{87}Sr/^{86}Sr ratio a function of the ^{88}Sr voltage showing an increase of the ^{87}Sr/^{86}Sr ratio with decreasing voltage.

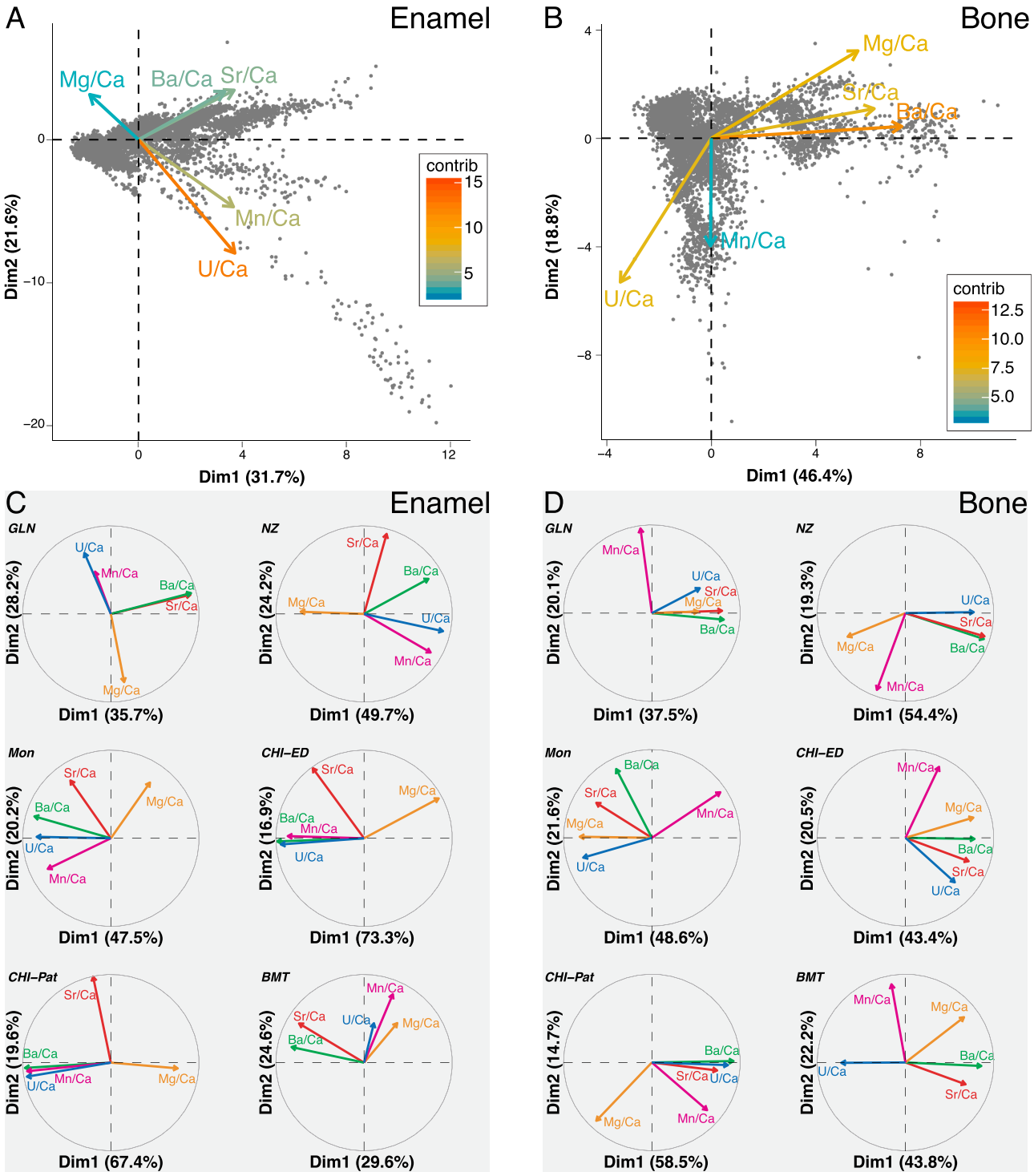

Fig. 3. Principal component analysis (PCA) of raw results. A) PCA of all enamel results. B) PCA of all bone results. C) PCA of enamel results for each locality. D) PCA of bone results for each locality.

inspection of the variance for a given location provides more complex results for enamel (Fig. 3C) and bone (Fig. 3D). Abbreviations of the archaeological sites are given in Table 1. For enamel, the Sr/Ca and Ba/Ca ratios are free of diagenesis at GLN and BMT, while low and high Mg/Ca ratio, respectively, is associated to high Mn/Ca and U/Ca ratios. At NZ, Mon, CHI-ED and CHI-Pat, the enamel Ba/Ca ratio has a diagenetic component because the Ba/Ca, Mn/Ca and U/Ca eigenvectors have closely related directions. In these sites, the enamel Sr/Ca ratio seems to be free of diagenetic influence. For bone, the Sr/Ca and Ba/Ca ratios have most often a diagenetic component, except at Mon, as illustrated by the common direction of the biogenic and diagenetic eigenvectors.

3.4. *Cleaning data from diagenesis and too low Sr content*

PCA indicates that diagenesis occurs on a site-by-site systematics and that the chemical composition of bone and enamel is differently affected by diagenesis. Analysis of the effects of diagenesis at the individual scale reveals even more complicated patterns. An example is provided for the

GLN-210 individual (Fig. 4A and B). Two diagenetic zones can be identified in enamel. In the diagenetic Zone 1, the increase of the Mn/Ca and U/Ca ratios is accompanied by a concomitant increase of the Ba/Ca ratio and of the Ca concentration, and a decrease of the Mg/Ca ratio (Fig. 4A). A simultaneous increase of the Sr/Ca ratio is less evident and is not associated to variations of the $^{87}Sr/^{86}Sr$ ratio anyway. The most likely explanation is that a Ca-rich, probably calcite, secondary phase precipitated in a crack of the enamel, as recognized earlier by Grün et al. (2008) to be a classic process. This secondary calcite was U- and Ba-rich, but Mg-poor, and has a comparable Sr concentration and isotopic composition than enamel. The crack was also filled with Mn-rich oxy-hydroxides. In the diagenetic Zone 2, a small increase of the U/Ca ratio,

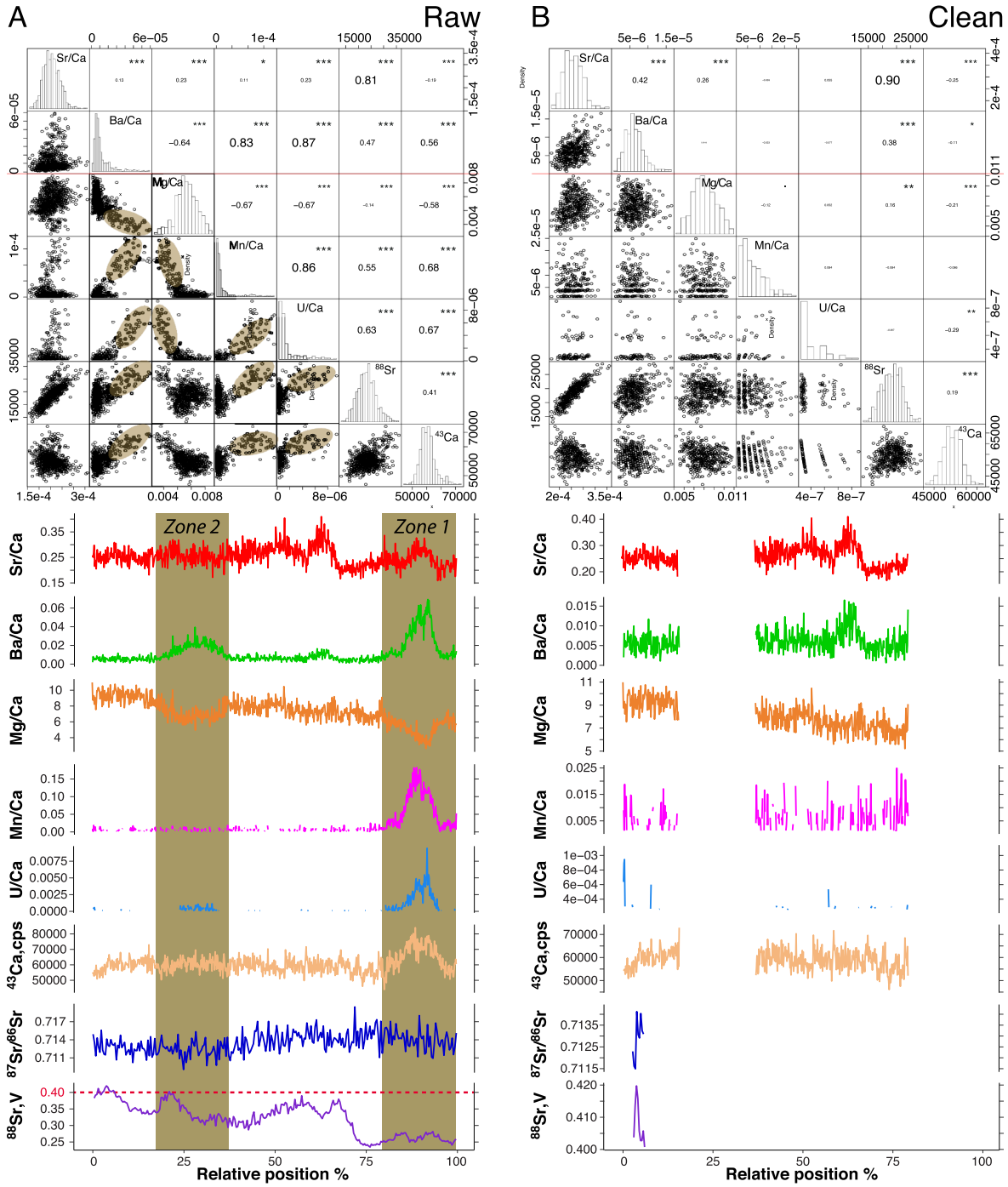

Fig. 4. Effect of cleaning the diagenetic overprinting. A) Chemical characterization of the raw sample. B) Chemical characterization of the clean sample. Each panel is composed of two parts. The top part is a correlation matrix which gives in the upper part the value of the Pearson correlation coefficient and the associated *P*value annotated with stars (*) as following: * *P*value < 0.05, ** *P*value < 0.001, *** *P*value $< 10^{-4}$, and in the lower part the scatterplot of the given association. The down part is composed of the rasters expressed in relative position to match elemental and isotopic profiles which had very different integration time, hence length. ^{43}Ca is reported to monitor potential Ca excess due to calcite incorporation. The areas where diagenesis is supposed to have occurred are highlighted in brown, and corresponding values are also highlighted in the scatterplots of the top part. The recognition and the extent of the supposed areas impacted by diagenesis has been done manually, and removed from the dataset, as well as $^{87}Sr/^{86}Sr$ values with a corresponding ^{88}Sr below 0.4 V. (For interpretation of the references to colour in this figure legend, the reader is referred to the web version of this article.)

but not of the Mn/Ca one, is associated to an increase of the Ba/Ca ratio and a decrease of the Mg/Ca ratio, without any change in the Sr/Ca ratio, Sr concentration nor isotopic composition (Fig. 4A). Here, U diffusion only cannot explain the observed diagenetic pattern because it would not take the associated Ba-enrichment and Mg-depletion into account. The observed diagenetic pattern is more likely explained by the presence of a secondary U-enriched phase, which must have been also Ba-enriched. The diagenetic effect on the Mg/Ca ratio is discussed in a subsequent section. The trace elements data were thus cleaned according to the following conditions: increase of the ^{43}Ca concentration or U/Ca or Mn/Ca ratios correlated to an increase of the Sr/Ca or Ba/Ca ratios or a decrease of the Mg/Ca ratio. The efficiency of the removing of the data suspected to be representative of a diagenetic process was globally followed using correlation matrix in which the lower half is filled with bivariate scatterplots (Fig. 4A and B). Highlighted are areas exhibiting diagenetic patterns (Fig. 4A) which are absent after the cleaning procedure (Fig. 4B). The procedure was done manually and checked iteratively. The cleaning procedure removed 24% of the original data. We observed that diagenesis occurs very often in the crj area, where the enamel is the thinnest. Regarding the accuracy of the ^{87}Sr/^{86}Sr ratio, all data with a^{88}Sr voltage below 0.4 V were removed (Fig. 4A and B). This procedure removed 76% of the original data. Reduced data are given in Table S1.

3.5. The case of Mg diagenesis

Magnesium is a bioessential element and as such, its concentration in the body is metabolically regulated to lie between the deficiency and toxicity thresholds. The concentration of Mg thus cannot be of any interest for tracing the consumption of Mg-enriched or Mg-depleted food items for paleodiet reconstructions (Klepingera, 1990; Reynard and Balter, 2014). However, the Mg stable isotope composition (δ^{26}Mg) of bone and tooth enamel is now recognized to vary according to the position of the animal in the trophic chain (Martin et al., 2014, 2015). It is therefore necessary to know how Mg behaves during diagenetic processes before using the Mg isotope compositions to paleontological applications. Lambert et al. (1985) measured the Mg concentration in a set of excavated bones and found higher values than in a reference set of modern bones. However, no information is available on the initial Mg concentration of the excavated bones. To the best of our knowledge, the results of the present study could the first robust evidence of Mg diagenesis in enamel. The example of the GLN-210 individual provided in Fig. 4 suggests that the Mg/Ca decreases when U/Ca increases, i.e., that Mg is leached out of enamel and bone during diagenesis. The Fig. 5 shows that this is a general pattern for the tooth enamel and bone samples analyzed here. Magnesium, as carbonate groups, represents defects in the hydroxyapatite (HAP) lattice, which decrease crystallinity and increase solubility (e.g., Laurencin et al., 2011; Legeros et al., 1996). Laurencin et al. (2011) also suggested, using Density Functional Theory calculations that a local clustering of Mg within the HAP lattice is likely to occur. A picture of Mg diagenesis in fossil HAP can be emphasized, which posits that Mg clusters, which are poorly crystallized, are likely to preferentially dissolve and react with the diagenetic fluids. The pending question, which requires further experiments, is whether the leaching of Mg is associated with an isotopic fractionation. If the leaching is quantitative, fossil bone and enamel would be Mg-depleted, but without Mg isotopic fractionation, allowing the analysis of accurate δ^{26}Mg values for paleontological studies.

3.6. Clean radiogenic Sr isotope and trace elements compositions

After cleaning the data, most of the samples exhibited truncated radiogenic Sr and trace elements profiles, so we calculated average and standard deviation for all parameters, which are given in Table S1. Cleaning the data has resulted in the identification of significant correlations among all averaged variables (Fig. 6A). These relationships are first discussed in bone and then in enamel.

3.6.1. Bone

Generally, bone ^{87}Sr/^{86}Sr ratios have local values (Fig. 6B), and the ^{87}Sr/^{86}Sr ratio is correlated with the Sr/Ca ratio (Fig. 6A), which would suggest that diagenesis is still overprinting the ^{87}Sr/^{86}Sr ratio (Budd et al., 2000). However, a close examination of the scatterplot between the ^{87}Sr/^{86}Sr and Sr/Ca ratios (Fig. 6C) shows that the human (GLN_221B), with the highest ^{87}Sr/^{86}Sr value and the lowest Sr/Ca ratio contributes to the observed correlation as an outlier. The observed correlation is also due to the higher Sr/Ca ratios of the BMT assemblage, which is composed of livestock remains only, which are known to be enriched relative humans thanks to the Ca biopurification process (Burton et al., 1999; Balter, 2004; Peek and Clementz, 2012). However, no human bone remains from BMT were analyzed so that the Ca biopurification process cannot be validated for this site. At GLN, where both human and faunal bone remains were analyzed, the Ca biopurification process between human and livestock exists but does not exhibit a typical bone Sr/Ca trophic Sr-enrichment of half a log unit (Fig. 6D, Balter, 2004), being closer to ~0.1. While humans have clearly lower

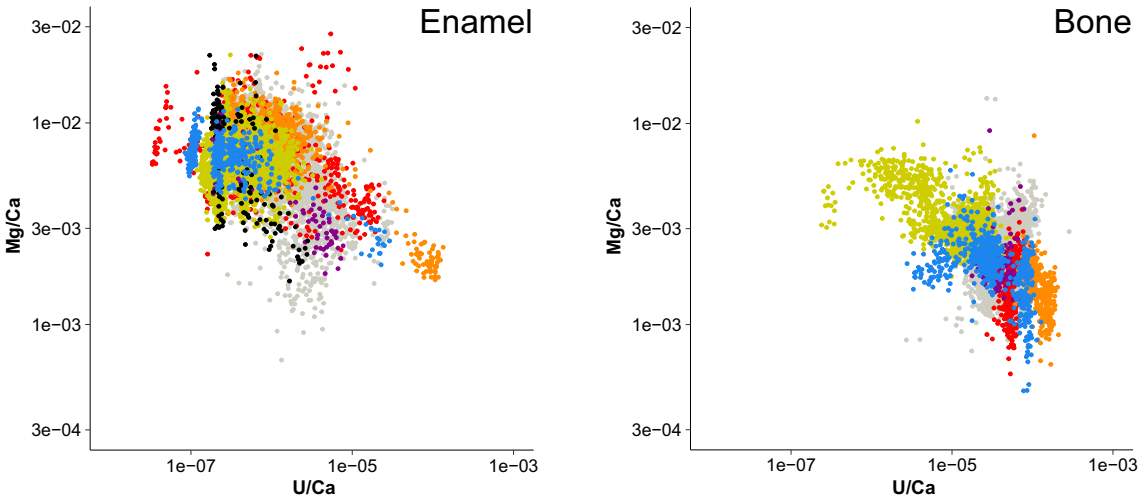

Fig. 5. Magnesium is leached during diagenesis. A) Scatterplot of the Mg/Ca ratio as a function of the U/Ca ratio in enamel. B) Scatterplot of the Mg/Ca ratio as a function of the U/Ca ratio in bone.

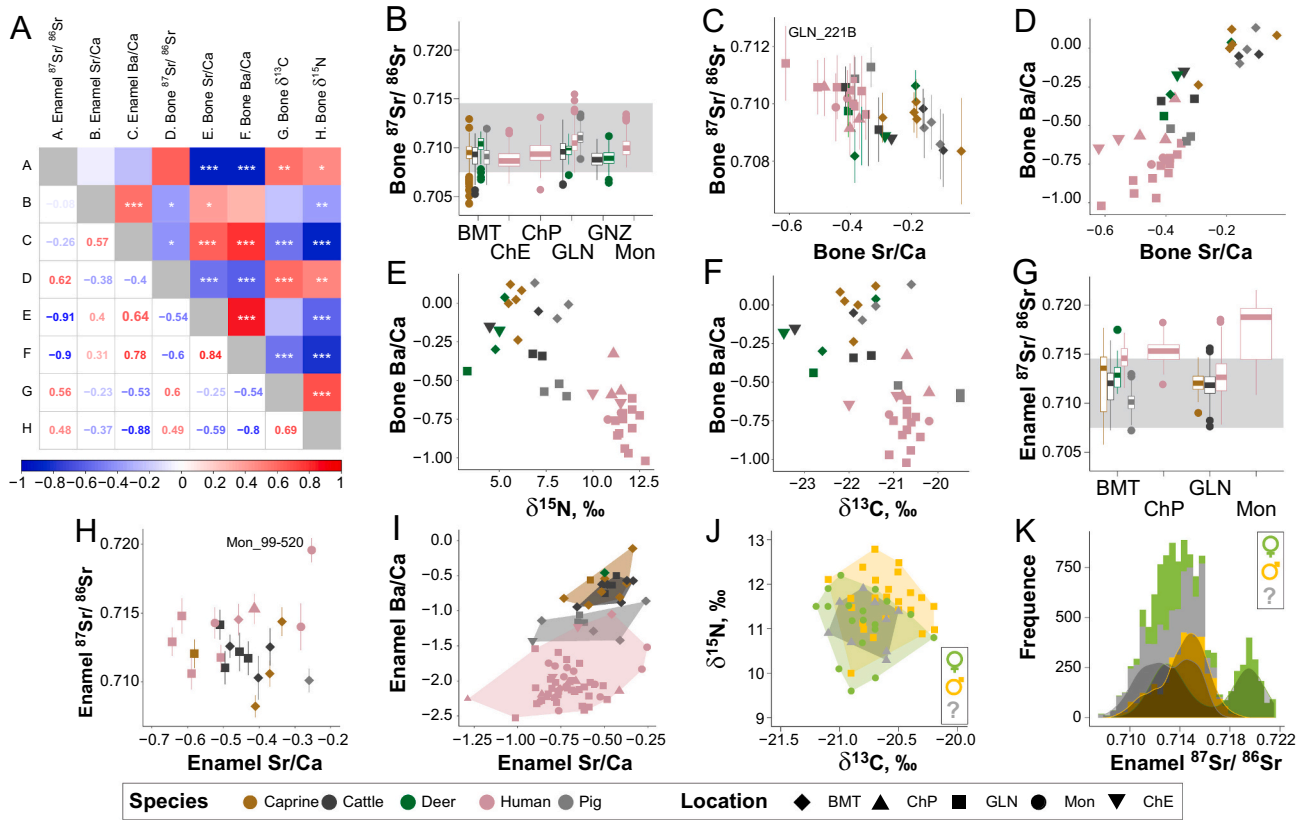

Fig. 6. Paleoecological and paleobiological significance of clean data. A) Correlation matrix for all clean results which gives in the lower part the Pearson correlation coefficient and in the upper part the associated *P*value annotated with stars (*) as following: * *P*value < 0.05, ** *P*value < 0.001, *** *P*value < 10^{-4}. B) Boxplot of all bone $^{87}Sr/^{86}Sr$ value for each locality. The gray area represents the local $^{87}Sr/^{86}Sr$ range. C) Scatterplot of bone average $^{87}Sr/^{86}Sr$ value as a function of bone average Sr/Ca ratio. D) Scatterplot of bone Ba/Ca ratio as a function of bone Sr/Ca ratio. E) Scatterplot of bone average Ba/Ca ratio as a function of bone $\delta^{15}N$ value. F) Scatterplot of bone average Ba/Ca ratio as a function of bone $\delta^{13}C$ value. G) Boxplot of all enamel $^{87}Sr/^{86}Sr$ values for each locality. The gray area represents the local $^{87}Sr/^{86}Sr$ range. H) Scatterplot of enamel average $^{87}Sr/^{86}Sr$ values as a function of enamel average Sr/Ca ratio. I) Scatterplot of enamel average Ba/Ca ratio as a function of enamel average Sr/Ca ratio. J) Scatterplot of bone $\delta^{15}N$ value as a function of bone $\delta^{13}C$ value. K) Histogram of the distribution of all cleaned enamel $^{87}Sr/^{86}Sr$ values according to sex. The curves represent density distribution for each sex. Ratios are expressed as log (Sr,Ba / Ca * 1000).

bone Ba/Ca than livestock at GLN (Fig. 6D, Wilcoxson, *P* value*** = 0.0004), the typical bone Ba/Ca trophic Ba-enrichment of one log unit is not preserved (it is rather close to ~0.5 at GLN, Fig. 6D). The bone biogenic Ba/Ca values seem however to be well-maintained as illustrated by the very good correlation with collagen $\delta^{15}N$ values, where human and livestock samples exhibit a species- and location-specific distribution (Fig. 6E). A distribution of the bone Ba/Ca and collagen $\delta^{13}C$ values according to species and location is also observed (Fig. 6F).

To summarize the results on bone, the overall picture argues for a diagenetic overprinting of Sr, but not Ba, despite the cleaning of the supposed diagenetic data. It is likely that part of the bone Sr burden supposedly cleaned from diagenesis is in fact overprinted by diagenesis in a pervasive way that could not be detectable by local disturbances as identified here with laser ablation in enamel. These results stress the importance of the leaching protocols for eliminating diagenetic compounds in fossil bone and conclude that bone is not a suitable material for laser ablation.

3.6.2. Enamel

The variability of the enamel $^{87}Sr/^{86}Sr$ ratios (Fig. 6G) is higher than in bone (Fig. 6B). Enamel $^{87}Sr/^{86}Sr$ ratios are not correlated to Sr/Ca ratios (Fig. 6H) and Sr and Ba are more depleted in enamel (Fig. 6I) than in bone (Fig. 6D). These first observations are in agreement with a lack of significant diagenetic effects on the original Sr and Ba contents (Budd et al., 2000; Peek and Clementz, 2012). In addition, while the Sr/Ca ratio exhibits a slight Sr-enrichment from human to livestock (~ 0.3 log unit), the Ba/Ca ratio has here the expected log unit (>1). These results are in agreement with previous studies (Sponheimer and Lee-Thorp, 2006; Tacail et al., 2019), confirm that the Sr/Ca ratio in enamel is a poor proxy of trophic level and validate that cleaned enamel has not been significantly altered by diagenesis. Noteworthy is the intermediate trophic position of pigs between bovids and humans (Fig. 6I). To summarize the results on enamel, the overall picture to argues for an absence of diagenetic overprinting of the $^{87}Sr/^{86}Sr$, Sr/Ca and Ba/Ca ratios, suggesting that the cleaning of the supposed diagenetic data has been efficient.

3.7. The context of the Neolithic revolution

Considering the geochemical differences highlighted for human and livestock among locations (Fig. 6E, F, I), it is likely that the Neolithic society was organized into small communities, managing their resources independently and locally, although probably exchanging people and goods with outside. For instance, the clear distinct bone Ba/Ca signatures between the livestock at BMT and GLN is a strong argument for specific livestock management, as it has already been proposed on the grounds of stable isotopes for these sites (Rey et al., 2019) or for other Neolithic sites (Oelze et al., 2011; Goude et al., 2019). Pending questions regarding livestock management are whether it was free-ranging and to what extent the livestock was allowed to range (e.g., Bickle and Hofmann, 2007). Here, livestock have local enamel $^{87}Sr/^{86}Sr$ ratios while humans have generally higher enamel $^{87}Sr/^{86}Sr$ ratios (Fig. 6F). This

seems to indicate that humans, during the formation of the M2 tooth, i.e., approximately between 2.5 and 8.5 ± 0.5 years old, included a non-local diet with high $^{87}Sr/^{86}Sr$ value, and were more mobile than the livestock. However, a close examination of the data reveals a more thorough pattern that cannot rule out the existence of micro-regional differences in the bioavailable Sr isotopic baseline. Indeed, some of human Sr isotope values come from MON and CHI-Pat for which there is no associated fauna. The human mobility, as recorded by the enamel $^{87}Sr/^{86}Sr$ ratio, is more likely due to practises unrelated to livestock herding.

One obvious $^{87}Sr/^{86}Sr$ outlier can be identified, i.e., Mon_99–520 (0.7196 ± 0.0018, ± 2SD, Fig. 6H), who is a female (Table S1). Differences in bone collagen for the $\delta^{13}C$ and $\delta^{15}N$ values are observed between males and females (Fig. 6J, MANOVA, *p*-value** = 0.0031), suggesting dietary sex-related differences (Rey et al., 2019). We thus performed histograms on enamel $^{87}Sr/^{86}Sr$ ratios according to sex (Fig. 6K). The distribution of the $^{87}Sr/^{86}Sr$ ratio is not statistically different between sexes (Student *t*-test, *p*-value = 0.61), but that of males seems to have higher $^{87}Sr/^{86}Sr$ values than of females in enamel (Fig. 6G). Interestingly, the distribution of the $^{87}Sr/^{86}Sr$ values for indeterminate is bimodal, suggesting that the sex difference of the $^{87}Sr/^{86}Sr$ is real. Despite the small number of samples having provided exploitable results (8 males and 4 females) and that sex differences should be considered in a site-by-site approach, this indicates a differential sex-related mobility pattern. The case of Mon 99–520 is interesting, because it suggests that this girl has grown in a very distinct area with a very high $^{87}Sr/^{86}Sr$ value, probably in the neighboring granitic Morvan area. Inclusion of foreign females in Neolithic group is a still debated question (e.g., Bentley et al., 2012; Goude et al., 2019, 2020; Rey et al., 2021), that could be further assessed by $^{87}Sr/^{86}Sr$ variation in enamel using laser ablation.

4. Concluding remarks

The laser ablation technique is capable to generate simple profiles of trace elements concentrations and radiogenic Sr isotope compositions in tooth enamel, but not in bone. In enamel, spatial variation not only allows the reconstruction of life traits histories such as diet and mobility, but also the identification of areas where diagenesis has left clues of modifications of the original signatures. Once identified, these areas can be withdrawn from the results. The identification of diagenetic areas in bone is more difficult, probably because the diffusion is higher than in enamel and hence contrasts with normal areas more attenuated. One disadvantage of laser ablation technique is that the sample cannot be cleaned from extraneous components using wet chemistry because the sample needs to be powdered. However, none of this prevents the possibility to soak the chip of fossil bone and tooth enamel in dilute acetic acid to remove surficial calcitic contaminants before laser ablation measurements. The efficiency of such a strategy could be evaluated by performing laser ablation profiles before and after the leaching pretreatment in further studies. Finally, to the best of our knowledge, the Laboratoire de Géologie de Lyon is the only lab that uses solid, homogeneous, matrix-matched, concentration-matched, and certified standard to correct for any interference of the $^{87}Sr/^{86}Sr$ ratios in Ca-phosphate samples analyzed by laser ablation. These standards can be shared on demand.

Declaration of Competing Interest

The authors declare that they have no known competing financial interests or personal relationships that could have appeared to influence the work reported in this paper.

Acknowledgement

The authors are very grateful to J.-B. Mallye and P. Magniez who provided anthropological material and related information for this study, G. Devilder for his assistance with the CAD and S. Ciliberto and V. Queste for the financial contribution of the Fonds Recherches of the Ecole Normale Supérieure de Lyon to the laser ablation device. This work was supported by the Institut Danone France/Fondation pour la Recherche Médicale 2015 partnership.

Appendix A. Supplementary data

Supplementary data to this article can be found online at https://doi.org/10.1016/j.chemgeo.2021.120608.

References

AlQahtani, S.J., Hector, M.P., Liversidge, H.M., 2010. Brief communication: the London atlas of human tooth development and eruption. Am. J. Phys. Anthropol. 142, 481–490.
Austin, C., Smith, T.M., Bradman, A., Hinde, K., Joannes-Boyau, R., Bishop, D., Hare, D. J., Doble, P., Eskenazi, B., Arora, M., 2013. Barium distributions in teeth reveal early-life dietary transitions in primates. Nature 498, 216–219.
Balter, V., 2004. Allometric constraints on Sr/Ca and Ba/Ca partitioning in terrestrial mammalian trophic chains. Oecologia 139, 83–88.
Balter, V., Lécuyer, C., 2004. Determination of Sr and Ba partitioning coefficients between apatite and water from 5°C to 60°C: a new thermometer for aquatic environments. Geochim. Cosmochim. Acta 68, 423–432.
Balter, V., Person, A., Labourdette, N., Drucker, D., Renard, M., Vandermeersch, B., 2001. Were Neandertalians essentially carnivores? Sr and Ba preliminary results of the mammalian palaeobiocoenosis of Saint-Césaire. C. R. Acad. Sci. Ser. IIA Earth Planet. Sci. 332, 59–65.
Balter, V., Saliège, J.F., Bocherens, H., Person, A., 2002. Evidence of physico–chemical and isotopic modifications in archaeological bones during controlled acid etching. Archaeometry 44, 329–336.
Balter, V., Telouk, P., Reynard, B., Braga, J., Thackeray, F., Albarède, F., 2008. Analysis of coupled Sr/Ca and 87Sr/86Sr variations in enamel using laser-ablation tandem quadrupole-multicollector ICPMS. Geochim. Cosmochim. Acta 72, 3980–3990.
Balter, V., Braga, J., Telouk, P., Thackeray, J.F., 2012. Evidence for dietary change but not landscape use in South African early hominins. Nature 489, 558–560.
Bentley, R.A., Bickle, P., Fibiger, L., Nowell, G.M., Dale, C.W., Hedges, R.E.M., Hamilton, J., Wahl, J., Francken, M., Grupe, G., Lenneis, E., Teschler-Nicola, M., Arbogast, R.-M., Hofmann, D., Whittle, A., 2012. Community differentiation and kinship among Europe's first farmers. Proc. Natl. Acad. Sci. 109, 9326–9330.
Bickle, P., Hofmann, D., 2007. Moving on: the contribution of isotope studies to the early Neolithic of Central Europe. Antiquity 81, 1029–1041.
Brazier, J.M., Schmitt, A.D., Pelt, E., Lemarchand, D., Gangloff, S., Tacail, T., Balter, V., 2020. R($^{87}Sr/^{86}Sr$) and $\delta^{88/86}Sr_{SRM987}$ values of mineral, vegetal and animal reference materials. Geostand. Geoanal. Res. 44, 331–348.
Budd, P., Montgomery, J., Barreiro, B., Thomas, R.G., 2000. Differential diagenesis of strontium in archaeological human dental tissues. Appl. Geochem. 15, 687–694.
Burton, J.H., Price, T.D., Middleton, W.D., 1999. Correlation of bone Ba/Ca and Sr/Ca due to biological purification of calcium. J. Archaeol. Sci. 26, 609–616.
Copeland, S.R., Sponheimer, M., le Roux, P.J., Grimes, V., Lee-Thorp, J.A., de Ruiter, D. J., Richards, M.P., 2008. Strontium isotope ratios (87Sr/86Sr) of tooth enamel: a comparison of solution and laser ablation multicollector inductively coupled plasma mass spectrometry methods. Rapid Commun. Mass Spectrom. 22, 3187–3194.
Dolphin, A.E., Goodman, A.H., Amarasiriwardena, D.D., 2005. Variation in elemental intensities among teeth and between pre- and postnatal regions of enamel. Am. J. Phys. Anthropol. 128, 878–888.
Gilbert, C., Sealy, J., Sillen, A., 1994. An Investigation of Barium, Calcium and Strontium as Palaeodietary Indicators in the Southwestern Cape, South Africa. J. Archaeol. Sci. 21, 173–184.
Goude, G., Salazar-García, D.C., Power, R.C., Terrom, J., Rivollat, M., Deguilloux, M.-F., Pemonge, M.-H., Le Bailly, M., Andre, G., Coutelas, A., Hauzeur, A., 2019. A Multidisciplinary Approach to Neolithic Life Reconstruction. J. Archaeol. Method Theory 26, 537–560.
Goude, G., Salazar-García, D.C., Power, R.C., Rivollat, M., Gourichon, L., Deguilloux, M.-F., Pemonge, M.-H., Bouby, L., Binder, D., 2020. New insights on Neolithic food and mobility patterns in Mediterranean coastal populations. Am. J. Phys. Anthropol. 173, 218–235.
Grün, R., Aubert, M., Joannes-Boyau, R.C., Moncel, M., 2008. High resolution analysis of uranium and thorium concentration as well as U-series isotope distributions in a Neanderthal tooth from Payre (Ardeche, France) using laser ablation ICP-MS. Geochim. Cosmochim. Acta 72, 5278–5290.
Hedges, R.E., Clement, J.G., Thomas, C.D., O'Connell, T.C., 2007. Collagen turnover in the adult femoral mid-shaft: modeled from anthropogenic radiocarbon tracer measurements. Am. J. Phys. Anthropol. 133, 808–816.
Hopkins, R.J.A., Snoeck, C., Higham, T.F.G., 2016. When dental enamel is put to the acid test: pretreatment effects and radiocarbon dating. Radiocarbon 58, 893–904.
Horstwood, M.S.A., Evans, J.A., Montgomery, J., 2008. Determination of Sr isotopes in calcium phosphates using laser ablation inductively coupled plasma mass spectrometry and their application to archaeological tooth enamel. Geochim. Cosmochim. Acta 72, 5659–5674.

Humphrey, L.T., Dean, M.C., Jeffries, T.E., Penn, M., 2008. Unlocking evidence of early diet from tooth enamel. Proc. Natl. Acad. Sci. 105, 6834–6839.
Joannes-Boyau, R., Adams, J.W., Austin, C., Arora, M., Moffat, I., Herries, A.I.R., Tonge, M.P., Benazzi, S., Evans, A.R., Kullmer, O., Wroe, S., Dosseto, A., Fiorenza, L., 2019. Elemental signatures of Australopithecus africanus teeth reveal seasonal dietary stress. Nature 572, 112–115.
Klepingera, L.L., 1990. Magnesium ingestion and bone magnesium concentration in paleodietary reconstruction: cautionary evidence from an animal model. J. Archaeol. Sci. 17, 513–517.
Kohn, M.J., Schoeninger, M.J., Barker, W.W., 1999. Altered states: Effects of diagenesis on fossil tooth chemistry. Geochim. Cosmochim. Acta 63, 2737–2747.
Kohn, M.J., Morris, J., Olin, P., 2013. Trace element concentrations in teeth – a modern Idaho baseline with implications for archeometry, forensics, and palaeontology. J. Archaeol. Sci. 40, 1689–1699.
Lambert, J.B., Vlasak, S., Simpson, Szpunar, Buikstra, J.E., 1985. Bone diagenesis and dietary analysis. J. Hum. Evol. 14, 477–482.
Laurencin, D., Almora-Barrios, N., de Leeuw, N.H., Gervais, C., Bonhomme, C., Mauri, F., Chrzanowski, W., Knowles, J.C., Newport, R.J., Wong, A., Gan, Z., Smith, M.E., 2011. Magnesium incorporation into hydroxyapatite. Biomaterials 32, 1826–1837.
Le Luyer, M., Coquerelle, M., Rottier, S., Bayle, P., 2016. Internal Tooth Structure and Burial Practices: insights into the Neolithic Necropolis of Gurgy (France, 5100-4000 cal. BC). PLoS One 11, e0159688.
Legeros, R.Z., Sakae, T., Bautista, C., Retino, M., Legeros, J.P., 1996. Magnesium and Carbonate in Enamel and Synthetic Apatites. Adv. Dent. Res. 10, 225–231.
Lugli, F., Cipriani, A., Peretto, C., Mazzucchelli, M., Brunelli, D., 2017. In situ high spatial resolution 87Sr/86Sr ratio determination of two Middle Pleistocene (c.a. 580ka) Stephanorhinus hundsheimensis teeth by LA–MC–ICP–MS. Int. J. Mass Spectrom. 412, 38–48.
Lugli, F., Cipriani, A., Capecchi, G., Ricci, S., Boschin, F., Boscato, P., Iacumin, P., Badino, F., Mannino, M.A., Talamo, S., Richards, M.P., Benazzi, S., Ronchitelli, A., 2019. Strontium and stable isotope evidence of human mobility strategies across the last Glacial Maximum in southern Italy. Nat. Ecol. Evol. 3, 905–911.
Martin, J.E., Vance, D., Balter, V., 2014. Natural variation of magnesium isotopes in mammal bones and teeth from two South African trophic chains. Geochim. Cosmochim. Acta 130, 12–20.
Martin, J.E., Vance, D., Balter, V., 2015. Magnesium stable isotope ecology using mammal tooth enamel. Proc. Natl. Acad. Sci. 112, 430–435.
Martin, J.E., Deesri, U., Liard, R., Wattanapituksakul, A., Suteethorn, S., Lauprasert, K., Tong, H., Buffetaut, E., Suteethorn, V., Suan, G., Télouk, P., Balter, V., 2016. Strontium isotopes reveal long-term residence of thalattosuchians in the freshwater environment. Paleobiology 42, 143–156.
Montgomery, J., Evans, J.A., Horstwood, M.S.A., 2010. Evidence for long-term averaging of strontium in bovine enamel using TIMS and LA-MC-ICP-MS strontium isotope intra-molar profiles. Environ. Archaeol. 15, 32–42.
Müller, W., Anczkiewicz, R., 2016. Accuracy of laser-ablation (LA)-MC-ICPMS Sr isotope analysis of (bio) apatite–a problem reassessed. J. Anal. At. Spectrom. 31, 259–269.
Müller, W., Fricke, H., Halliday, A.N., McCulloch, M.T., Wartho, J.-A., 2003. Origin and migration of the alpine iceman. Science 302, 862–866.
Müller, W., Nava, A., Evans, D., Rossi, P.F., Alt, K.W., Bondioli, L., 2019. Enamel mineralization and compositional time-resolution in human teeth evaluated via histologically-defined LA-ICPMS profiles. Geochim. Cosmochim. Acta 255, 105–126.
Nelson, B.K., Deniro, M.J., Schoeninger, M.J., De Paolo, D.J., Hare, P.E., 1986. Effects of diagenesis on strontium, carbon, nitrogen and oxygen concentration and isotopic composition of bone. Geochim. Cosmochim. Acta 50, 1941–1949.
Oelze, V.M., Siebert, A., Nicklisch, N., Meller, H., Dresely, V., Alt, K.W., 2011. Early Neolithic diet and animal husbandry: stable isotope evidence from three Linearbandkeramik (LBK) sites in Central Germany. J. Archaeol. Sci. 38, 270–279.
Peek, S., Clementz, M.T., 2012. Ontogenetic variations in Sr/Ca and Ba/Ca ratios of dental bioapatites from Bos taurus and Odocoileus virginianus. J. Trace Elem. Med. Biol. 26, 248–254.
Rey, L., Tacail, T., Le Luyer, M., Salazar-Garcìa, D.C., Balter, V., Rottier, S., Goude, G., 2016. Tracking male vs. female Neolithic behaviors: a new multi-element and multi-isotope-ratio analysis to reconstruct diet and mobility in northern France. In: 8th World Archaeological Congress, Kyoto (Japan).
Rey, L., Goude, G., Rottier, S., 2017. Comportements alimentaires au Néolithique : nouveaux résultats dans le Bassin parisien à partir de l'étude isotopique (δ13C, δ15N) de la nécropole de Gurgy « Les Noisats » (Yonne, Ve millénaire av. J.-C.). Bull. Mém. Soc. Anthropol. Paris 29, 54–69.
Rey, L., Salazar-García, D.C., Chambon, P.h., Santos, F., Rottier, S., Goude, G., 2019. A multi-isotope analysis of Neolithic human groups in the Yonne valley, Northern France: insights into dietary patterns and social structure. Archaeol. Anthropol. Sci. 11, 5591–5616.
Rey, L., Rottier, S., Santos, F., Goude, G., 2021. Sex and age-related social organization in the Neolithic: a promising survey from the Paris Basin. J. Archaeol. Sci. Rep. 38, 103092.
Reynard, B., Balter, V., 2014. Trace elements and their isotopes in bones and teeth: Diet, environments, diagenesis, and dating of archeological and paleontological samples. Palaeogeogr. Palaeoclimatol. Palaeoecol. 416, 4–16.
Sillen, A., Balter, V., 2018. Strontium Isotopic aspects of *Paranthropus robustus* teeth; Implications for habitat, residence, and growth. J. Hum. Evol. 114, 118–130.
Sillen, A., Hall, G., Richardson, S., Armstrong, R., 1998. 87Sr/86Sr ratios in modern and fossil food-webs of the Sterkfontein Valley: implications for early hominid habitat preference. Geochim. Cosmochim. Acta 62, 2463–2473.
Simonetti, A., Buzon, M.R., Creaser, R.A., 2008. In-situ elemental and Sr isotope investigation of human tooth enamel by laser ablation-(MC)-ICP-MS: Successes and pitfalls. Archaeometry 50, 371–385.
Sponheimer, M., Lee-Thorp, J.A., 2006. Enamel diagenesis at South African Australopith sites: Implications for paleoecological reconstruction with trace elements. Geochim. Cosmochim. Acta 70, 1644–1654.
Szulc, P., Seeman, E., Delmas, P.D., 2000. Biochemical Measurements of Bone turnover in Children and Adolescents. Osteoporos. Int. 11, 281–294.
Tacail, T., Télouk, P., Balter, V., 2016. Precise analysis of calcium stable isotope variations in biological apatites using laser ablation MC-ICPMS. J. Anal. At. Spectrom. 31, 152–162.
Tacail, T., Kovačiková, L., Brůžek, J., Balter, V., 2017. Spatial distribution of trace element Ca-normalized ratios in primary and permanent human tooth enamel. Sci. Total Environ. 603-604, 308–318.
Tacail, T., Martin, J., Arnaud-Godet, F., Thackeray, F., Cerling, T., Braga, J., Balter, V., 2019. Calcium isotopic patterns in enamel reflect different nursing behaviors among South African early hominins. Sci. Adv. 5 eaax3250.
Willmes, M., McMorrow, L., Kinsley, L., Armstrong, R., Aubert, M., Eggins, S., Falguères, C., Maureille, B., Moffat, I., Grün, R., 2013. The IRHUM (Isotopic Reconstruction of Human Migration) database - bioavailable strontium isotope ratios for geochemical fingerprinting in France. Earth Syst. Sci. Data Discuss. 6, 761–777.
Willmes, M., Kinsley, L., Moncel, M.H., Armstrong, R.A., Aubert, M., Eggins, S., Grün, R., 2016. Improvement of laser ablation in situ micro-analysis to identify diagenetic alteration and measure strontium isotope ratios in fossil human teeth. J. Archaeol. Sci. 70, 102–116.